GaAs/AlAs triple-coupled cavity with InAs quantum dots for ultrafast wavelength conversion devices

Xiangmeng Lu*, Hiroto Ota, Naoto Kumagai†, Takahiro Kitada, and Toshiro Isu

Graduate School of Science and Technology, Tokushima University, Tokushima 770-8506, Japan

*E-mail: xm-lu@tokushima-u.ac.jp

†Present address: National Institute of Advanced Industrial Science and Technology (AIST), Tsukuba, 305-8506, Japan

We have investigated a GaAs/AlAs triple-coupled multilayer cavity structure with InAs quantum dots for an ultrafast wavelength conversion device. Three cavity modes with the resonance frequencies ω_1, ω_2, and ω_3 were used for efficient wavelength conversion via a four-wave mixing (FWM) process. Identical frequency separation between two adjacent modes ($\omega_1 - \omega_2 = \omega_2 - \omega_3$) was successfully realized using a controlled lateral thickness variation across the wafer. Time-resolved FWM signals from the triple-coupled multilayer cavity were measured using 100 fs laser pulses. The incident laser pulses were divided into two pulses and each of them was spectrally shaped individually so that the input and control pulses only covered the ω_1 and ω_2 modes, respectively. The wavelength-converted FWM signal with a frequency of ω_3 ($= 2\omega_2 - \omega_1$) was clearly observed when the sample was simultaneously irradiated with the input and control laser pulses.

1. Introduction

Four-wave mixing (FWM) in a nonlinear optical medium is one of the promising methods for all-optical wavelength conversion in advanced wave division multiplexing (WDM) networks. Regarding the development of reliable and format-transparent conversion devices, there have been many reports on all-optical wavelength conversion via a nonlinear FWM process in semiconductor optical amplifiers (SOAs),[1-4] Si waveguides,[5,6] and highly nonlinear fibers.[7,8] In addition, all-optical logic gates based on FWM in SOAs have been demonstrated for optical quadrature phase-shift keying (QPSK) signals.[9]

Optical nonlinear phenomena in semiconductor vertical microcavities are very interesting and useful for constructing all-optical devices for dense parallel processing because the optical axis of the incident light is perpendicular to the wafer surface. We have demonstrated optical Kerr gate switches based on a GaAs/AlAs multilayer cavity with InAs quantum dots (QDs) embedded in strain-relaxed barriers.[10-15] The strong internal light electric field due to the cavity effects markedly enhances of nonlinear phase shift in the half-wavelength ($\lambda/2$) cavity layer containing QDs. Vertical geometry all-optical switches based on the reflectance modulation of conventional InAs QDs placed in a GaAs/AlAs multilayer cavity have also been demonstrate by Jin and coworkers.[16,17] A coupled cavity system has a unique feature of multiple cavity modes providing a new functionality.

In our recent studies, strong sum frequency generation[18-20] and difference frequency generation (DFG) in the terahertz region[21-24] were successfully demonstrated by the simultaneous excitation of two cavity modes in a coupled multilayer cavity structure. We have also proposed a GaAs/AlAs triple-coupled multilayer cavity structure for novel ultrafast wavelength conversion devices operating in the 1.5 μm waveband for

telecommunication systems.[25] Three cavity modes with the optical frequencies ω_1, ω_2, ω_3 are realized in the triple-coupled cavity structure that consists of three cavity layers with the same effective optical thickness. The frequency separation between two adjacent modes is identical, that is, $\omega_1 - \omega_2 = \omega_2 - \omega_3$. When two laser pulses with the frequencies ω_1 and ω_2 are simultaneously incident to the triple-coupled cavity structure, an FWM signal with $2\omega_2 - \omega_1$ should be efficiently generated because $2\omega_2 - \omega_1$ is coincident with the other mode frequency of ω_3. We found that wavelength-converted FWM signals showed a lower intensity than degenerate FWM signals. The reason for this was that $2\omega_2 - \omega_1$ was not exactly coincident with ω_3 results from the slight variation of the cavity mode frequency caused by the layer-to-layer thickness variation due to slight and gradual changes in Ga and Al fluxes during molecular beam epitaxy (MBE). Therefore, the precise control of the cavity modes is important for obtaining stronger frequency conversion signals. Another significant improvement in the wavelength conversion is also expected by introducing good nonlinear materials into a λ/2 cavity. One of the good candidate materials is an ensemble of InAs QDs having a resonance energy near the cavity mode wavelengths. We have demonstrated the enhancement of the optical Kerr signal from the cavity with InAs QDs compared with that without QDs.[26]

Using improved techniques, we have investigated the FWM in a GaAs/AlAs triple-coupled cavity with 3.4 ML InAs QDs, which were embedded in a strain-relaxed $In_{0.35}Ga_{0.65}As$ layer to extend the resonance wavelength above 1.5 μm.[27] An equivalent effective optical thickness of three cavity layers was realized using a controlled lateral thickness variation across the wafer. Degenerate FWM signals with ω_1 and ω_2 were clearly observed when incident pulses covered both ω_1 and ω_2 frequencies. However, no wavelength-converted FWM signal with ω_3 (= $2\omega_2 - \omega_1$) was observed. The possible

reason for this is that the absorption of wavelength-converted signals by QDs is more significant than that of degenerate FWM signals.

In this study, we grew a GaAs/AlAs coupled multilayer cavity with 2.7 ML InAs QDs having no absorption around the cavity mode wavelength of 1.5 μm. We investigated the frequency separations of cavity modes depending on the cavity layer thickness using reflection spectra. We obtained a cavity with an equivalent optical thickness of three cavity layers, which demonstrated that $\omega_1 - \omega_2 = \omega_2 - \omega_3$. The tripled-coupled cavity structure was grown by MBE and time-resolved FWM measurements were performed using spectrally shaped laser pulses to observe wavelength conversion.

2. Epitaxial growth by MBE

The GaAs/AlAs triple-coupled multilayer cavity structure with InAs QDs shown in Fig. 1 was grown on a 2 inch GaAs substrate by MBE. After the growth of buffer layers containing an AlAs/$Al_{0.5}Ga_{0.5}As$ (5 nm/100 nm) etch stopper structure, which is essential for the selective removal of the GaAs substrate,[28] 12-period and 8.5-period GaAs/AlAs (111 nm/130 nm) DBRs were used for the series connection of three GaAs 2λ cavity layers. Nine layers of self-assembled InAs QDs (2.7 ML) were inserted only in the topside GaAs 2λ cavity. The photoluminescence (PL) of QDs was examined and it had a peak wavelength of around 1.2 μm that inhibited absorption around the cavity mode wavelength of 1.5 μm. The substrate rotation was stopped twice during the growth of the topside GaAs 2 λ cavity to form a controlled lateral thickness variation across the wafer.

3. Reflection spectra at various positions

An equivalent optical thickness of three cavity layers is desirable for obtaining stronger frequency conversion signals. Since the materials of the bottom and middle cavity layers are different from that of the top cavity layer in this structure, it is difficult to grow three cavity layers whose effective optical thicknesses were exactly the same over the entire wafer. Fortunately, an equivalent optical thickness of three cavity layers can be partially realized using the thickness distribution in a wafer by the growth without the substrate rotation. Figure 2 shows optical reflection spectra measured at various wafer positions. Three reflection dips at approximately 1.5 μm correspond to the cavity modes whose frequencies depend on the measurement position. The lateral thickness variation of one of the three cavity layers causes slight variations of three cavity mode frequencies (ω_1, ω_2, and ω_3) in the 2 inch wafer. The same frequency separation (18 nm) between two adjacent modes was obtained. These results indicate that a triple-coupled multilayer cavity structure with nine layers of InAs QDs, which has an equivalent effective optical thickness of three cavity layers, was successfully fabricated.

4. Time-resolved FWM measurements

Time-resolved FWM measurements were performed after removing the substrate to eliminate signal generation in the thick substrate. Before the substrate removal, the sample was mounted on a 1-mm-thick glass substrate using optical adhesive (Norland 83H). After curing by UV light, the sample was mechanically polished to thin the GaAs substrate to approximately 20 μm. The remaining substrate was then completely removed by selective wet etching using a citric acid-based etchant.[28)] Finally, the sample was dipped in a buffered hydrogen fluoride (BHF) solution to remove the oxide layer.

Figure 3 shows the experimental setup for time-resolved FWM measurements using a femtosecond laser system with a 100 kHz repetition rate. All measurements were performed at room temperature. The laser pulses were initially divided into two pulses by a polarizing beam splitter for use as input and control pulses of FWM signal generation. Then, each pulse was spectrally shaped by a spectral width restriction (SWR) system[29] that consists of a slit between a pair of gratings and cylindrical lenses. Using the two SWR systems, the input pulse contained the ω_1 frequency component without covering the ω_2 and ω_3 modes, whereas the control pulse contained the ω_2 component without covering ω_1 and ω_3 modes. The relative delay time (Δt) of the input pulse was introduced using a mechanical delay stage and the input pulse beam was chopped at 400 Hz for standard lock-in detection. Both pulses were linearly polarized in the same direction and they were focused on the sample surface as shown in Fig. 3(b). Here, the wavevectors of the input and control pulses are denoted by $\mathbf{k}_a$ and $\mathbf{k}_b$, respectively. To detect only the FWM signal with the wavevector of $2\mathbf{k}_b - \mathbf{k}_a$, which was spatially separated from the input and control pulses[30], a small aperture was placed between the collimating lens and the cooled InGaAs photodiode (PD) detector. The spectrum at a fixed delay time was also measured using a spectrometer with a cooled InGaAs PD array. A flip mirror was placed in the optical path of the FWM signal to measure either the temporal profile or the signal spectrum.

4.1 FWM measurements without SWR

Let us first examine the FWM signal measured without SWR, which was performed by removing the slit between a pair of gratings and cylindrical lenses in each SWR system of Fig. 3(a). Figure 4(a) shows the optical transmission spectrum measured in the normal incidence configuration using a pulse laser after removing the GaAs substrate. Transmission

peaks ($\omega_1, \omega_2,$ and ω_3) corresponding to the three cavity modes were clearly observed. The shape of the transmission spectrum depended on the shape of the incident pulse and it was not normalized here. Figures 4(b) and 4(c) show the spectra of the incident pulse and FWM signal at $\Delta t = 0$ ps, respectively. As shown in Figs. 4(a) and 4(b), the incident pulse entirely covered the two modes of ω_1 and ω_2, while the ω_3 mode was only slightly covered in the long-wavelength tail. We clearly observed an FWM signal whose frequency was outside the incident pulse range, in addition to the degenerate FWM signals of the two cavity modes with the frequencies ω_1 (= $2\omega_1$ - ω_1) and ω_2 (= $2\omega_2$ - ω_2). This indicates that frequency conversion was achieved using the three cavity modes of a triple-coupled cavity with QDs. The peak frequency of the additional FWM signal corresponds to that of the other mode ω_3, with a significant peak observed on the long wavelength side. The vertical dashed line in Fig. 4 indicates the position of $2\omega_2$ - ω_1, where the signal peak is expected for wavelength conversion through the FWM process. $2\omega_2$ - ω_1 was exactly coincident with ω_3 in this sample; therefore, a high-efficiency wavelength conversion signal $2\omega_2$ - ω_1 was realized. However, the detected wavelength-converted signal $2\omega_2$ - ω_1 might mixed up with a certain degenerate FWM signal ω_3 (= $2\omega_3$ - ω_3) because the ω_3 mode was slightly covered by the incident pulse as indicated in Fig. 4(b).

Figure 5 shows the Δt-dependent FWM signal measured using laser pulses, which is also shown in Fig. 4(b). The three different frequency components of the FWM signal can be seen in Fig. 4(c). Since each component was generated through the coherent FWM process, the interference between the three components caused a clear oscillating temporal profile as shown in Fig. 5. When the delay time was around zero, the envelope of the oscillating profile rose and decayed exponentially. The rise and decay times were about 0.4 and 0.8 ps, respectively, indicating an ultrafast FWM response.

4.2 FWM measurements with SWR

To exclude the degenerate FWM signal ω_3 (= $2\omega_3$ - ω_3), let us next investigate the FWM signal measured using two SWR systems. In this case, the input pulse only covers the ω_1 mode while the control pulse only covers the ω_2 mode as shown in Fig. 6(b). The transmission spectrum is shown once again in Fig. 6(a) for better readable. Figures 6(c) and 6(d) show the measured spectra of the spatially separated FWM signal at Δt = -2 and 0 ps, respectively. In this measurement configuration, ω_1 and ω_2 peaks should not be observed at Δt = 0 ps because the degenerate FWM signals of the input and control pulses cannot be detected according to the momentum conservation law. Moreover, considering the temporal profile in Fig. 5, ω_1 and ω_2 peaks should not be observed at Δt = -2 ps. Therefore, the measured ω_1 and ω_2 peaks were considered to originate from input and control pulse beams that scattered from the sample surface that might be rough owing to sample preparation. On the other hand, the ω_3 (= $2\omega_2$ - ω_1) peak was observed only when Δt = 0 ps. These results indicate that the wavelength conversion via FWM was successfully realized using three cavity modes in the triple-coupled coupled multilayer cavity containing InAs QDs. The clear wavelength-converted FWM signal in this study indicates that the absorption of FWM signals was inhibited by using InAs QDs with a PL peak wavelength of 1.2 μm, which was away from a cavity mode wavelength of around 1.5 μm. The wavelength-converted FWM signal could be further enhanced by tuning the resonance energy of QDs closer to the cavity mode wavelengths to obtain a larger nonlinear response with the precondition that there is no absorption of FWM signals.

5. Conclusions

We grew a GaAs/AlAs triple-coupled multilayer cavity with nine layers of InAs QDs for an ultrafast wavelength conversion device operating in the 1.5 μm waveband for telecommunication systems. We measured slight variations of three cavity mode frequencies (ω_1, ω_2, and ω_3) in a 2 inch wafer caused by a controlled lateral thickness variation due to the growth without substrate rotation. Identical frequency separation ($\omega_1 - \omega_2 = \omega_2 - \omega_3$) between two adjacent modes was realized, indicating that the GaAs/AlAs triple-coupled multilayer cavity with InAs QDs with an equivalent optical thickness of three cavity layers was successfully fabricated. Time-resolved FWM signals from the triple-coupled cavity were measured using 100 fs laser pulses. Incident laser pulses were divided into two pulses, which were spectrally shaped individually so that the input and control pulses only covered the ω_1 and ω_2 modes, respectively. The wavelength-converted FWM signal with the frequency ω_3 ($= 2\omega_2 - \omega_1$) was clearly observed.

Acknowledgment

This work was partly supported by a Grant-in-Aid for Scientific Research (B) (No. 24360028) from the Japan Society for the Promotion of Science (JSPS).

References

1) G. Contestabile, Y. Yoshida, A. Maruta, and K. Kitayama, IEEE Photonics Technol. Lett. **25**, 791 (2013).
2) C. Meuer, C. Schmidt-Langhorst, H. Schmeckebier, G. Fiol, D. Arsenijevic, C. Schubert, and D. Bimberg, Opt. Express **19**, 3788 (2011).
3) D. Nielsen, S. L. Chuang, N. J. Kim, D. Lee, S. H. Pyun, W. G. Jeong, C. Y. Chen, and T. S. Lay, Appl. Phys. Lett. **92**, 10 (2008).
4) T. Akiyama, H. Kuwatsuka, N. Hatori, Y. Nakata, H. Ebe, and M. Sugawara, IEEE Photonics Technol. Lett. **14**, 1139 (2002).
5) M. Pu, H. Hu, C. Peucheret, H. Ji, M. Galili, L.K. Oxenløwe, P. Jeppesen, J.M. Hvam, and K. Yvind, Opt. Express **20**, 16374 (2012).
6) H. Rong, Y.-H. Kuo, A. Liu, M. Paniccia, and O. Cohen, Opt. Express **14**, 1182 (2006).
7) J. Ma, J. Yu, C. Yu, Z. Jia, X. Sang, Z. Zhou, T. Wang, and G.K. Chang, J. Lightwave Technol. **24**, 2851 (2006).
8) K. Inoue, J. Lightwave Technol. **12**, 1916 (1994).
9) D. Kong, Y. Li, H. Wang, X. Zhang, J. Zhang, J. Wu, and J. Lin, IEEE Photonics Technol. Lett. **24**, 988 (2012).
10) T. Kitada, T. Kanbara, K. Morita, and T. Isu, Appl. Phys. Express **1**, 92302 (2008).
11) K. Morita, T. Takahashi, T. Kitada, and T. Isu, Appl. Phys. Express **2**, 82001 (2009).
12) T. Takahashi, T. Mukai, K. Morita, T. Kitada, and T. Isu, Jpn. J. Appl. Phys. **49**, 04DG02 (2010).
13) K. Morita, T. Takahashi, T. Kanbara, S. Yano, T. Mukai, T. Kitada, and T. Isu, Physica E **42**, 2505 (2010).

14) H. Ueyama, T. Takahashi, Y. Nakagawa, K. Morita, T. Kitada, and T. Isu, Jpn. J. Appl. Phys. **51**, 04DG06 (2012).

15) K. Morita, H. Ueyama, Y. Yasunaga, Y. Nakagawa, T. Kitada, and T. Isu, Jpn. J. Appl. Phys. **52**, 04CG04 (2013).

16) C. Y. Jin, O. Kojima, T. Kita, O. Wada, M. Hopkinson, and K. Akahane, Appl. Phys. Lett. **95**, 10 (2009).

17) C. Y. Jin, O. Kojima, T. Inoue, T. Kita, O. Wada, M. Hopkinson, and K. Akahane, IEEE J. Quantum Electron. **46**, 1582 (2010).

18) F. Tanaka, T. Takahashi, K. Morita, T. Kitada, and T. Isu, Jpn. J. Appl. Phys. **49**, 04DG01 (2010).

19) K. Morita, F. Tanaka, T. Takahashi, T. Kitada, and T. Isu, Appl. Phys. Express **3**, 72801 (2010).

20) F. Tanaka, T. Takimoto, K. Morita, T. Kitada, and T. Isu, Jpn. J. Appl. Phys. **50**, 04DG03 (2011).

21) K. Morita, S. Katoh, T. Takimoto, F. Tanaka, Y. Nakagawa, S. Saito, T. Kitada, and T. Isu, Appl. Phys. Express **4**, 102102 (2011).

22) S. Katoh, T. Takimoto, Y. Nakagawa, K. Morita, T. Kitada, and T. Isu, Jpn. J. Appl. Phys. **51**, 04DG05 (2012).

23) T. Kitada, S. Katoh, T. Takimoto, Y. Nakagawa, K. Morita, and T. Isu, IEEE Photonics J. **5**, 6500308 (2013).

24) T. Kitada, S. Katoh, T. Takimoto, Y. Nakagawa, K. Morita, and T. Isu, Appl. Phys. Lett. **102**, 251118 (2013).

25) T. Kitada, Y. Yasunaga, Y. Nakagawa, K. Morita, and T. Isu, Appl. Phys. Lett. **103**, 101109 (2013).

26) T. Kitada, T. Kanbara, S. Yano, K. Morita, and T. Isu, Jpn. J. Appl. Phys. **48**, 80203 (2009).

27) M. Ogarane, Y. Yasunaga, Y. Nakagawa, K. Morita, T. Kitada, and T. Isu, Jpn. J. Appl. Phys. **34**, 04DG05 (2015).

28) T. Kanbara, S. Nakano, S. Yano, K. Morita, T. Kitada, and T. Isu, Jpn. J. Appl. Phys. **48**, 04C105 (2009).

29) K. Morita, T. Takahashi, T. Kitada, and T. Isu, Jpn. J. Appl. Phys. **50**, 04DG02 (2011).

30) Y. Yasunaga, H. Ueyama, K. Morita, T. Kitada, and T. Isu, Jpn. J. Appl. Phys. **52**, 2 (2013).

Figure Captions

Fig. 1. (Color Online) Structure of the GaAs/AlAs triple-coupled multilayer cavity with InAs quantum dots.

Fig. 2. (Color Online) Reflection spectra measured at various positions of the epitaxial wafer.

Fig. 3. (Color Online) (a) Schematic illustration of experimental setup for FWM measurements. (b) Measurement configuration for spatially separated FWM signal $2\mathbf{k}_b$-$\mathbf{k}_a$ from the input and control pulses.

Fig. 4. (Color Online) (a) Transmission spectrum measured in the normal incidence configuration. (b) Spectrum of the incident pulse without SWR system. (c) Spectrum of FWM signal measured at $\Delta t = 0$ ps.

Fig. 5. (Color Online) Temporal profile of FWM signal measured without SWR system.

Fig. 6. (Color Online) (a) Transmission spectrum measured in the normal incidence configuration. (b) Spectra of input and control pulses with SWR systems. Spectra of FWM signal measured at (c) $\Delta t = -2$ ps and (d) $\Delta t = 0$ ps.

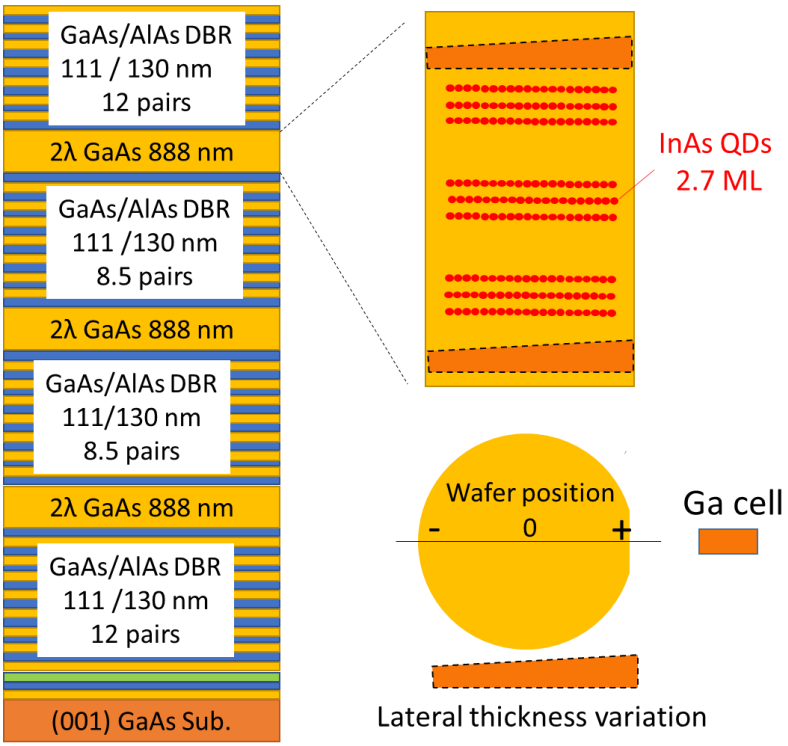

Fig. 1. (Color Online) Structure of the GaAs/AlAs triple-coupled multilayer cavity with InAs quantum dots.

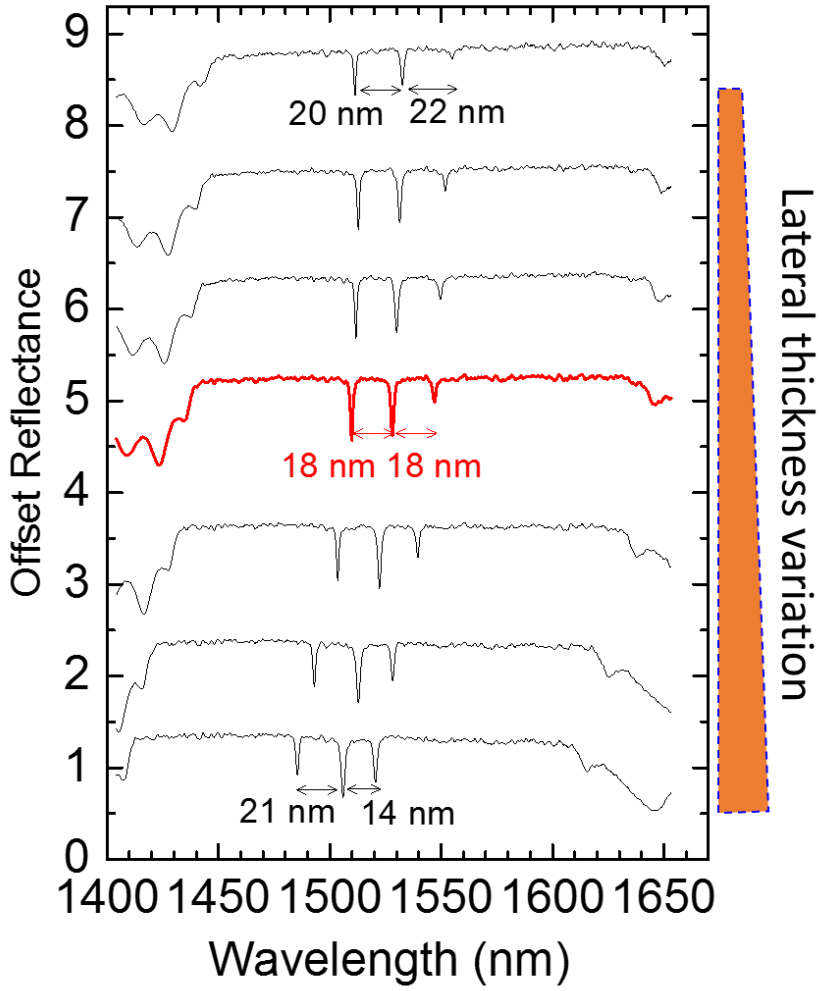

Fig. 2. (Color Online) Reflection spectra measured at various positions of the epitaxial wafer.

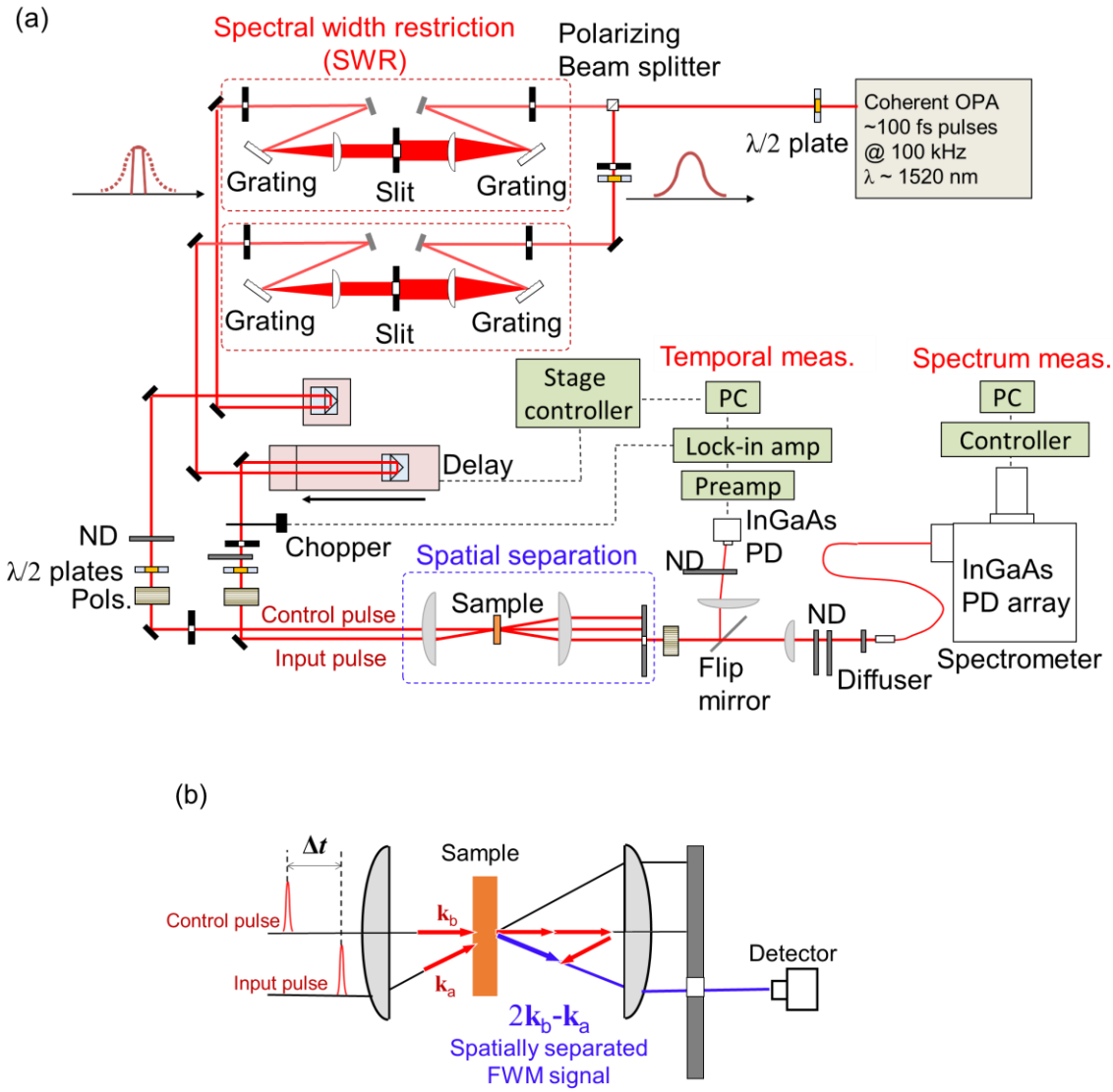

Fig. 3. (Color Online) (a) Schematic illustration of experimental setup for FWM measurements. (b) Measurement configuration for spatially separated FWM signal $2\mathbf{k}_b$-$\mathbf{k}_a$ from the input and control pulses.

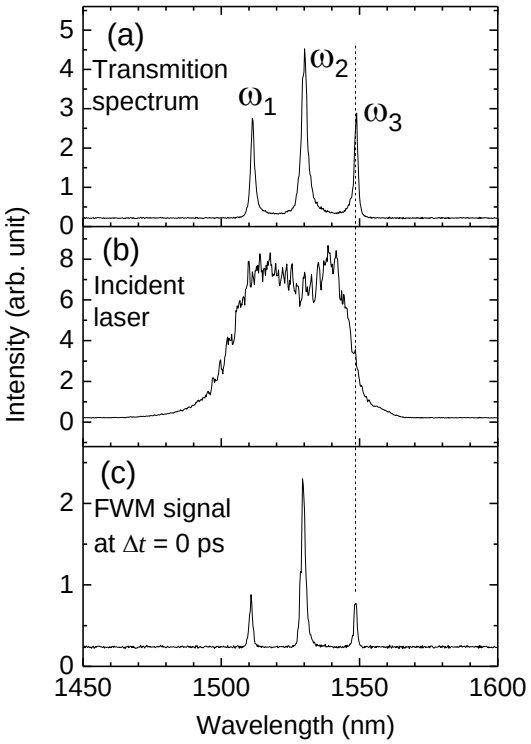

Fig. 4. (Color Online) (a) Transmission spectrum measured in the normal incidence configuration. (b) Spectrum of the incident pulse without SWR system. (c) Spectrum of FWM signal measured at $\Delta t = 0$ ps.

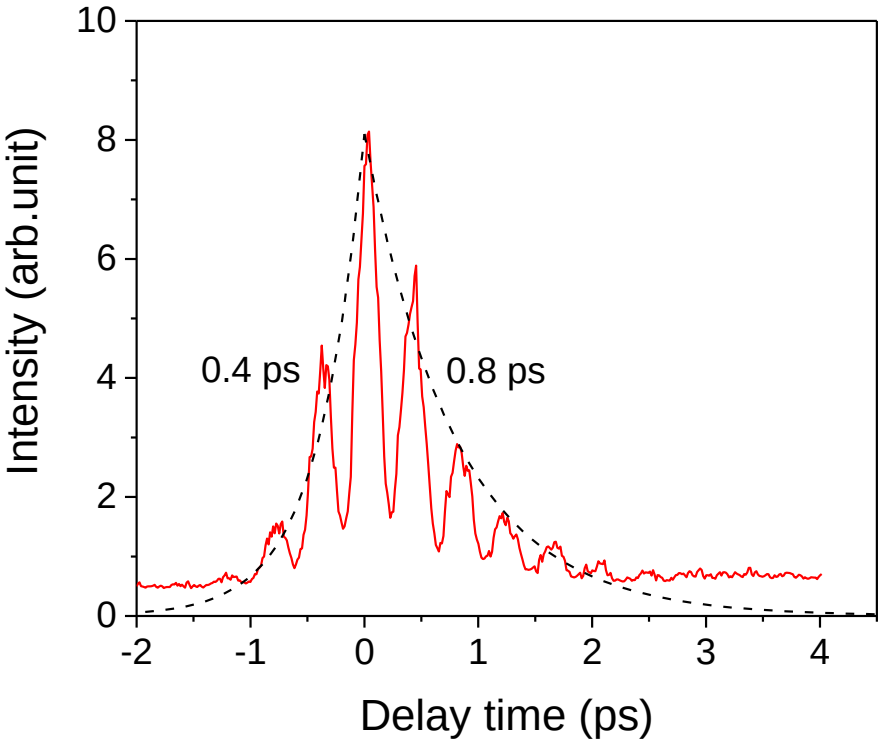

Fig. 5. (Color Online) Temporal profile of FWM signal measured without SWR system.

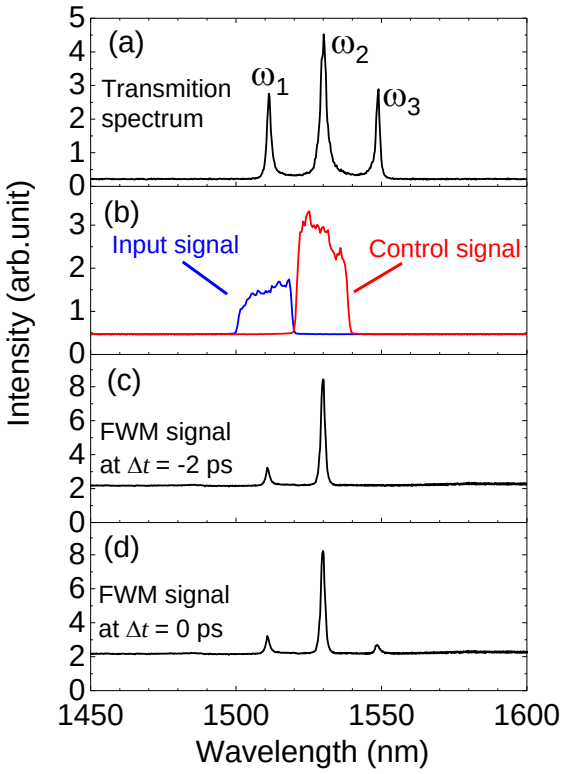

Fig. 6. (Color Online) (a) Transmission spectrum measured in the normal incidence configuration. (b) Spectra of input and control pulses with SWR systems. Spectra of FWM signal measured at (c) Δt = -2 ps and (d) Δt = 0 ps.